# Surface Chemistry of Gold Nanoparticles Mediates Their Exocytosis in Macrophages

**Nuri Oh[†,‡] and Ji-Ho Park[†,‡,§,*]**

[†]Department of Bio and Brain Engineering, [‡]Institute for Optical Science and Technology, and [§]Institute for the Nanocentury, Korea Advanced Institute of Science and Technology (KAIST), Daejeon 305-701, Republic of Korea

**ABSTRACT** Significant quantities of synthetic nanoparticles circulating in the body are cleared and retained for long periods of time in the resident macrophages of the mononuclear phagocytic system (MPS), increasing the likelihood of nanoparticle-mediated chronic toxicity. To date, there has been limited effort to understand how these nanoparticles leave the macrophages. Here, we demonstrate that the native surface chemistries of gold nanoparticles (GNPs) and their subsequent opsonization by serum proteins play critical roles in the exocytosis patterns in macrophages. The cationic GNPs were retained in the cells for a relatively long time, likely due to their intracellular agglomeration. In contrast, the PEGylated GNPs migrated in the cytoplasm in the form of individual particles and exited the cells rapidly because the PEG coating mitigated interactions between GNPs and intracellular proteins. Additionally, their exocytosis pattern was not significantly governed by the size, particularly in the range from 10 to 40 nm. These results suggest that systemic excretion and toxicity of nanoparticles cleared in the MPS could be modulated by engineering their surface chemistry.

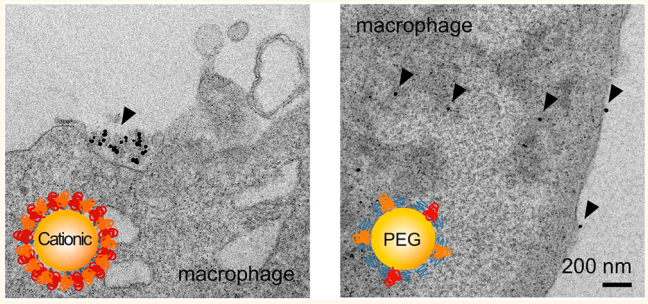


**KEYWORDS:** exocytosis · gold nanoparticle · macrophage · nanotoxicity · surface chemistry

Synthetic nanoparticles engineered for systemic administration into the body have great potential for detection and treatment of complex human diseases.[1,2] Despite significant effort to improve their targeting capability, significant quantities of nanoparticles in circulation are eventually cleared by the mononuclear phagocytic system (MPS),[3−10] part of the immune system consisting of phagocytic cells. Among various MPS cell types, the Kupffer cells of the liver and red pulp macrophages of the spleen play major roles in clearing, processing, and degrading the nanoparticles. Opsonin proteins in the blood rapidly adsorb to the nanoparticle surface, forming a protein corona.[11−14] Opsonin-coated nanoparticles are then recognized and taken up by MPS cells, and finally trapped in the lysosomes for a relatively long period, depending on their physicochemical properties.[4,5,7,8] Such long retention times increase the likelihood of nanoparticle-mediated chronic toxicity in the MPS *via* inflammation or immunological responses.[4,15,16] Thus, assessing the fate of nanoparticles in the resident macrophages of the MPS is important to clarify their *in vivo* potential toxicity.

Much progress has been made in understanding the size, shape, and surface chemistry effects of non-biodegradable nanoparticles on macrophage endocytosis.[17−21] Nanoparticles smaller than 100 nm reportedly enter macrophages by macropinocytosis, or scavenger receptors.[20,22−24] However, relatively little attention has been given to how these nanoparticles leave the macrophages, *i.e.*, the mechanism behind systemic excretion.[5,25−27] Various nanoparticle formulations, such as polymeric nanoparticles,[28−30] gold nanoparticles,[31−35] carbon nanotubes[36,37] metal oxide nanoparticles,[38,39] quantum dots,[40−42] mesoporous silica nanoparticles,[43,44] and nanodiamonds,[45] have been tested to characterize their exocytosis in many types of cells, primarily cancer cells; these studies yielded several important findings: nanoparticle exocytosis is an energy-dependent process and is influenced by nanoparticle size, surface chemistry, shape,

* Address correspondence to jihopark@kaist.ac.kr.

Received for review March 26, 2014 and accepted May 16, 2014.

**Published online May 16, 2014**
**10.1021/nn501668a**

and cell type. However, to our knowledge, only two brief reports have investigated the exocytosis of surface-tailored nanoparticles in macrophages.[15,38] Fischer *et al.* examined the exocytosis of surface-functionalized quantum dots (QD) in primary murine Kupffer cells for ~400 min; however, this time was too short to observe complete excretion of the intracellular QDs.[15] Serda *et al.* also examined the surface chemistry-dependent exocytosis of magnetic nanoparticles (MNP) delivered into murine macrophages by porous silicon microcarriers; the native surface properties of MNPs embedded in the microcarriers were secured during cellular uptake.[38] This outcome is different from that observed in *in vivo* situations, in which the nanoparticles are usually coated with serum proteins prior to cellular uptake. Thus, more systematic investigation is essential to better clarify their exocytosis process in MPS-associated macrophages.

Cellular uptake and biodistribution of gold-based nanomaterials have been extensively investigated in terms of their biosafety, due to their tremendous potential in medical applications (*e.g.*, gold salts approved for rheumatoid arthritis therapies[46]).[18,31,47−50] However, lack of knowledge about how the MPS rids itself of these nanoparticles has impeded their clinical translation. Particularly in the liver, these nanoparticles must escape macrophages and migrate to hepatocytes to be excreted through the hepatobiliary system. Their long-term retention in macrophages has been shown to induce inflammation and apoptosis in the liver.[4] Although several studies have demonstrated hepatobiliary clearance of systemically injected gold-based nanomaterials over the long-term,[6,51,52] none have reported complete excretion of the nanomaterial from the MPS within a reasonable period of time (excretion percentage: ~50% of poly(ethylene glycol) (PEG)ylated gold nanorods at two months post-injection,[6] and ~10% of anionic gold nanoparticles at six months post-injection[51]). We believe that the potential for *in vivo* toxicity from gold-based nanomaterials could be reduced if they are designed to efficiently facilitate exocytosis of the MPS macrophages. Thus, we systematically assessed the effect of size and surface chemistry of monodisperse gold nanoparticles (GNPs) on exocytosis patterns in macrophages *in vitro*. This exocytosis mechanism in macrophages is discussed here in an effort to elucidate it and thereby improve efficiency.

## RESULTS AND DISCUSSION

To engineer the design parameters for efficient exocytosis in macrophages, GNPs with various sizes and surface chemistries were prepared (Figure 1). We were particularly interested in studying the cellular fate of GNPs smaller than 50 nm, because smaller sizes are favorable for systemic injection. Citrate-coated GNPs (average sizes: ~10, 20, and 40 nm) were synthesized using a previously established method,[53] and used as anionic GNPs. Zwitterionic and PEGylated GNPs were then prepared by coating the citrated GNPs with cysteine and methoxy-PEG (mPEG)-sulfhydryl (2k) molecules, respectively. Cysteamine-coated GNPs (average sizes: ~10, 20, and 40 nm) were also synthesized for cationic GNPs using methods specified in previous studies.[54,55] Subsequently, all GNP formulations were coated with serum proteins prior to macrophage treatment, to mimic the opsonization process in blood circulation (Figure 1a). Transmission electron microscopy (TEM) revealed that all GNP formulations were fairly spherical with uniform diameters (Figure 1b and Supporting Information Figure S1). The average hydrodynamic diameters (HD) were slightly larger than the diameters observed using TEM, because TEM images did not reveal the organic-molecule coating (Figure 1c). The zeta potential results prior to serum coating well reflected the characterizations of the organic coatings. After serum coating, the HDs of all GNP formulations increased (regardless of their initial size) by ~10 nm for PEGylated GNPs, ~15 nm for cationic GNPs, and ~20 nm for other GNPs. Gel electrophoresis and thermogravimetric analysis (TGA) results, with proteins eluted from the GNPs, also supported the surface chemistry dependency on serum protein adsorption (Supporting Information Figure S2), which is in accordance with previous findings.[56,57] Zeta potential measurements revealed an anionic surface charge ranging from −40 to −15 mV for all GNP formulations, regardless of their original charge, reflecting the charges of the adsorbed proteins.[56] The protein coating can also cause a slight shift in the absorption spectra to longer wavelengths by ~5 nm. The PEGylated surface exhibited the lowest protein adsorption, as described in previous reports.[58,59]

Aggregated or agglomerated forms of nanoparticles influence their endocytosis patterns.[49] In this study, we focused on the exocytosis of GNPs taken up by macrophages in the form of individual particles. To determine whether the serum-coated GNPs were stable under the given test conditions, their HD and absorption spectra were monitored for 6 h (the incubation time for their endocytosis in the following experiments) in serum-free media at 37 °C using a dynamic light scattering (DLS) instrument and an ultraviolet−visible (UV/vis) spectrometer, respectively. The shift and broadening of the absorption spectrum indicate their aggregation/agglomeration.[49] The HDs and absorption spectra of the GNP formulations did not change significantly (Supporting Information Figures S3 and S4), suggesting that no aggregation or agglomeration occurred during the incubation period. Thus, our experimental setup allowed single serum-coated GNPs to interact with macrophages *in vitro*.

Systemically administered nanoparticles interact with circulating monocytes and eventually accumulate

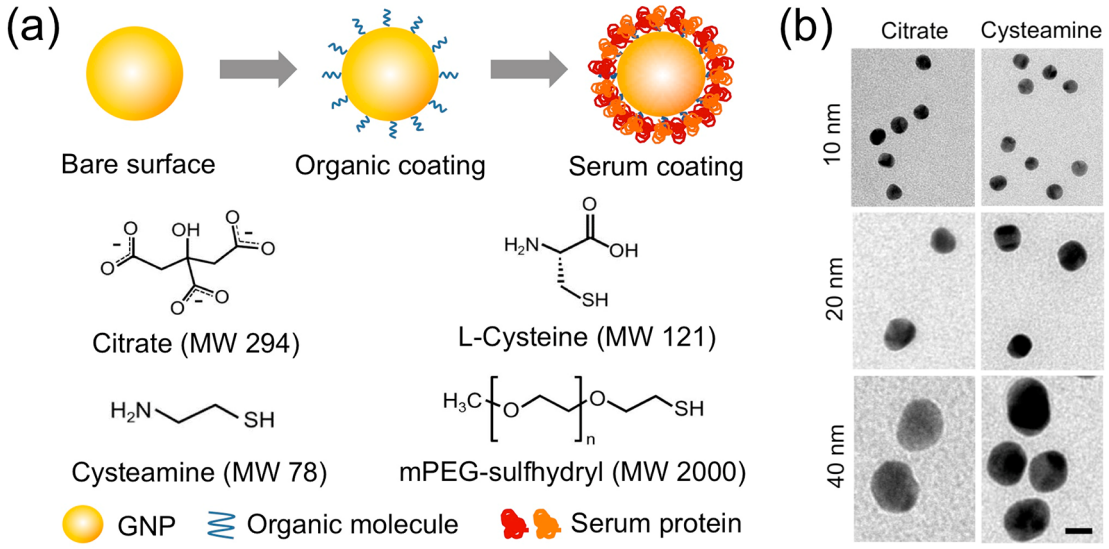


(c)

| Sample | | | Before protein coating | | | After protein coating | | |
|---|---|---|---|---|---|---|---|---|
| NP | Surface | TD (nm) | HD (nm) | ZP (mV) | Peak (nm) | HD [% increase] (nm) | ZP (mV) | Peak (nm) |
| G10A | Anionic | 10.52 ± 0.72 | 14.41 ± 1.61 | -29.28 ± 1.28 | 520 | 36.03 ± 1.51 [150 %] | -28.39 ± 1.91 | 525 |
| G10C | Cationic | 9.43 ± 0.98 | 13.48 ± 0.29 | 26.33 ± 1.98 | 520 | 30.64 ± 2.52 [127 %] | -20.09 ± 0.76 | 525 |
| G10Z | Zwitterionic | | 16.26 ± 2.27 | -0.92 ± 0.53 | 520 | 36.12 ± 2.34 [122 %] | -21.27 ± 1.63 | 525 |
| G10P | PEGylated | | 25.42 ± 1.25 | -27.54 ± 2.65 | 525 | 37.22 ± 1.87 [ 46 %] | -29.61 ± 2.57 | 530 |
| G20A | Anionic | 20.05 ± 0.12 | 26.86 ± 1.85 | -38.40 ± 1.09 | 525 | 48.22 ± 1.22 [ 80 %] | -40.01 ± 2.37 | 530 |
| G20C | Cationic | 19.95 ± 0.28 | 29.02 ± 2.80 | 47.12 ± 3.12 | 525 | 40.79 ± 1.48 [ 41 %] | -23.58 ± 1.45 | 530 |
| G20Z | Zwitterionic | | 27.23 ± 3.02 | 0.12 ± 2.72 | 525 | 47.51 ± 0.93 [ 74 %] | -15.56 ± 1.72 | 530 |
| G20P | PEGylated | | 35.93 ± 1.31 | -13.55 ± 2.54 | 530 | 44.09 ± 1.31 [ 23 %] | -34.74 ± 1.69 | 535 |
| G40A | Anionic | 40.45 ± 3.36 | 45.49 ± 1.22 | -35.5 ± 2.34 | 535 | 66.28 ± 2.09 [ 46 %] | -36.45 ± 2.63 | 540 |
| G40C | Cationic | 42.45 ± 2.64 | 47.79 ± 1.64 | 40.03 ± 2.46 | 535 | 62.31 ± 0.98 [ 30 %] | -22.07 ± 1.86 | 540 |
| G40Z | Zwitterionic | | 48.84 ± 0.46 | 0.13 ± 1.61 | 535 | 65.38 ± 1.99 [ 34 %] | -25.89 ± 0.78 | 540 |
| G40P | PEGylated | | 55.15 ± 0.91 | -15.18 ± 3.25 | 540 | 66.02 ± 1.54 [ 20 %] | -30.98 ± 1.11 | 545 |

**Figure 1. Preparation and characterization of serum-coated gold nanoparticles. (a) Coating procedure of gold nanoparticles (GNPs). Citrate-coated GNPs with averages sizes of ~10, 20, and 40 nm were first synthesized and used as anionic GNPs. Zwitterionic and PEGylated GNPs were then prepared by coating the citrated ones with cysteine and mPEG-sulfhydryl (2k) molecules, respectively. Cysteamine-coated GNPs were also synthesized for cationic ones. Subsequently, all GNP formulations were further coated with serum proteins prior to treating macrophages. (b) Transmission electron microscopic images of citrate- (left) and cysteamine-coated (right) GNPs with average diameters of ~10 (top), 20 (middle), and 40 nm (bottom). Scale bar is 20 nm. (c) Characterization of surface-functionalized GNPs before and after serum coating. The number after the G (GNP identifier) designates the size. The letters A, C, Z, and P indicate anionic, cationic, zwitterionic, and PEGylated surface, respectively. The physical diameters (TEM diameter (TD)) were determined from the images obtained with TEM ($n$ = 10). The hydrodynamic diameters (HD) and zeta potentials (ZP) were determined based on dynamic light scattering (DLS) measurements ($n$ = 3). The peak represents the maximum peak of absorption spectrum of GNPs. All data of TD, HD, and ZP are means ± SD ($n$ = 3).**

in the resident macrophages of the MPS. Thus, we first evaluated the endocytosis of various GNP formulations in both monocytes and macrophages, before assessing their subsequent exocytosis. Human macrophage-like U937 cells were selected as the MPS macrophage model, because these are capable of efficient phagocytosis of foreign materials.[60−64] Undifferentiated (monocytes) or phorbol-12-myristate-13-acetate (PMA)-differentiated U937 cells (macrophages) were treated with each formulation of serum-coated GNPs for 6 h in serum-supplemented media at 37 °C to saturate their endocytosis.[19,20,28] The quantities of GNPs taken up by cells 6-h post-treatment were measured using inductively coupled plasma mass spectrometry (ICP-MS). Dark field microscopy (DFM) was used to visualize the cellular uptake with the strong scattering property. The scattering signal can be also used to estimate the aggregated state of GNPs in the cells; aggregated GNPs appear as orange-red and single GNPs appear as green-yellow.[65] Only a small amount of GNP formulations was observed in the monocytes, although cationic GNPs exhibited a relatively higher cellular uptake (Figure 2a,c). ICP-MS results revealed that in the macrophages, cellular uptake of cationic GNPs was higher

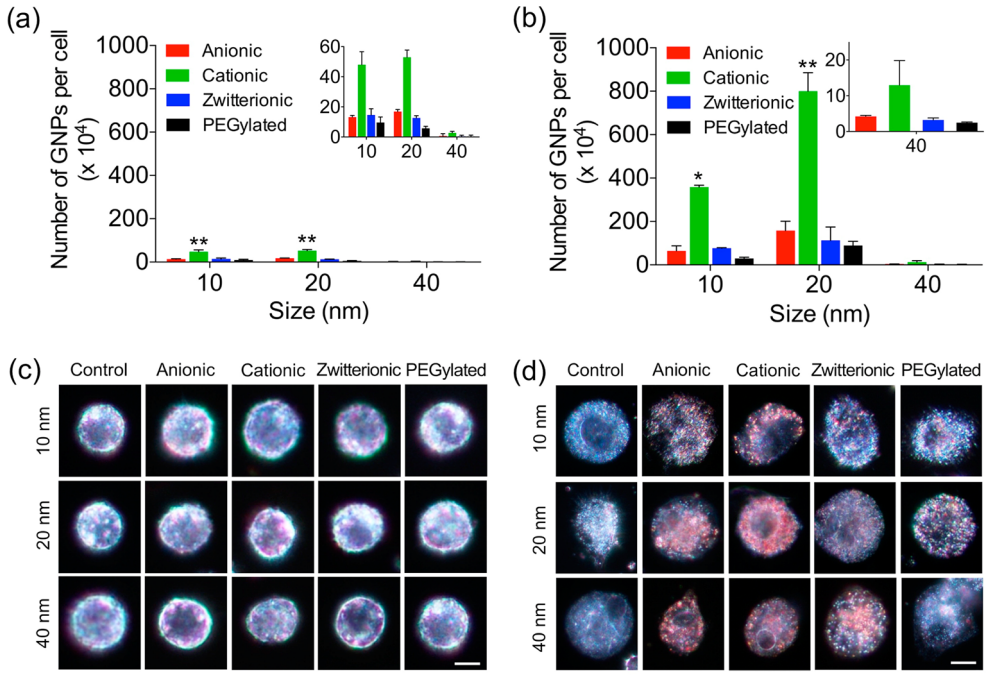


**Figure 2. Endocytosis of serum-coated gold nanoparticles in monocytes and macrophages. (a and b) Amount of gold nanoparticles (GNPs) taken up by monocytes (a) and macrophages (b). The amount of intracellular GNPs was determined by ICP-MS after the cells were treated with GNPs for 6 h. (c and d) Dark field microscopic images of serum-coated GNPs taken up by monocytes (c) and macrophage (c). The intracellular GNPs were imaged using a dark field microscope after the cells were treated with GNPs for 6 h. Scale bars indicate 10 $\mu$m. Data represent means $\pm$ SD ($n = 3$, *$p < 0.05$, and **$p < 0.01$, analyzed by two-way analysis of variance, followed by Bonferroni test).**

than that of other GNPs, regardless of their size (Figure 2b). Our results also demonstrated that the PMA-differentiated U937 cells preferentially internalized the 20 nm-diameter GNPs, compared with the 10 and 40 nm GNPs. Moreover, DFM images displayed significantly more orange-red dots in the cells treated with cationic GNPs, compared with those having other GNPs; this indicated the presence of aggregated GNPs, presumably in the endosomes and lysosomes (Figure 2d), supporting the ICP-MS results. In contrast, PEGylated GNPs were inefficient in entering the macrophages; the internalized ones appeared as yellowish dots in DFM images, indicating their intracellular retention in the form of individual particles. Collectively, these results suggest that the native surface properties of GNPs, which would be associated with type and quantity of adsorbed serum proteins *via* hydrophobic or electrostatic interactions, primarily determine their endocytotic fate.

Most of the nanoparticles taken up by macrophages undergo translocation from endosomes to lysosomes,[66,67] where they are further processed for digestion. However, to date, few studies have investigated the exocytotic fate of non-biodegradable nanoparticles. We next examined how the size and surface chemistry of GNPs mediated serum protein adsorption, subsequent endocytosis, and eventual exocytosis in macrophages. PMA-differentiated U937 cells were treated with each formulation of GNPs for 6 h in serum-supplemented media at 37 °C, and were then extensively washed to remove any weakly bound GNPs on the plasma membrane; the samples were further incubated for 48 h in GNP-free serum-supplemented media. To measure the quantity of GNPs exocytosed from the cells, supernatants were collected over a 48-h post-incubation period, and the amount of Au ions in the supernatants was analyzed using ICP-MS. The resulting exocytosis pattern represented the percentage of GNPs that remained in the macrophages at each time point after incubation in the GNP-free media. Our results demonstrated that, regardless of size, cationic GNPs remained in cells longer than any other formulations, while PEGylated GNPs exhibited the highest rate of exocytosis (Figure 3a–c). Previous finding also revealed that cationic (polyethylenimine-coated) nanoparticles (diameter: ~130 nm) were exocytosed more slowly in cancer cells, compared with anionic (phosphate-modified) ones.[44] For internalized cationic GNPs with diameters of ~10, 20, and 40 nm, 25.01, 20.32, and 37.30%, respectively, were extracellularly released within 48 h. In contrast, 83.34, 71.65, and 81.08% of intracellular PEGylated GNPs with diameters of ~10, 20, and 40 nm, respectively, underwent exocytosis within 48 h. The anionic and zwitterionic GNPs exhibited medium exocytosis rates between those of PEGylated and cationic ones. Additionally, it was unlikely that their exocytosis patterns were influenced by the size range tested here (10–40 nm) (Supporting Information Figure S5), indicating that surface properties of the GNPs are a more dominant

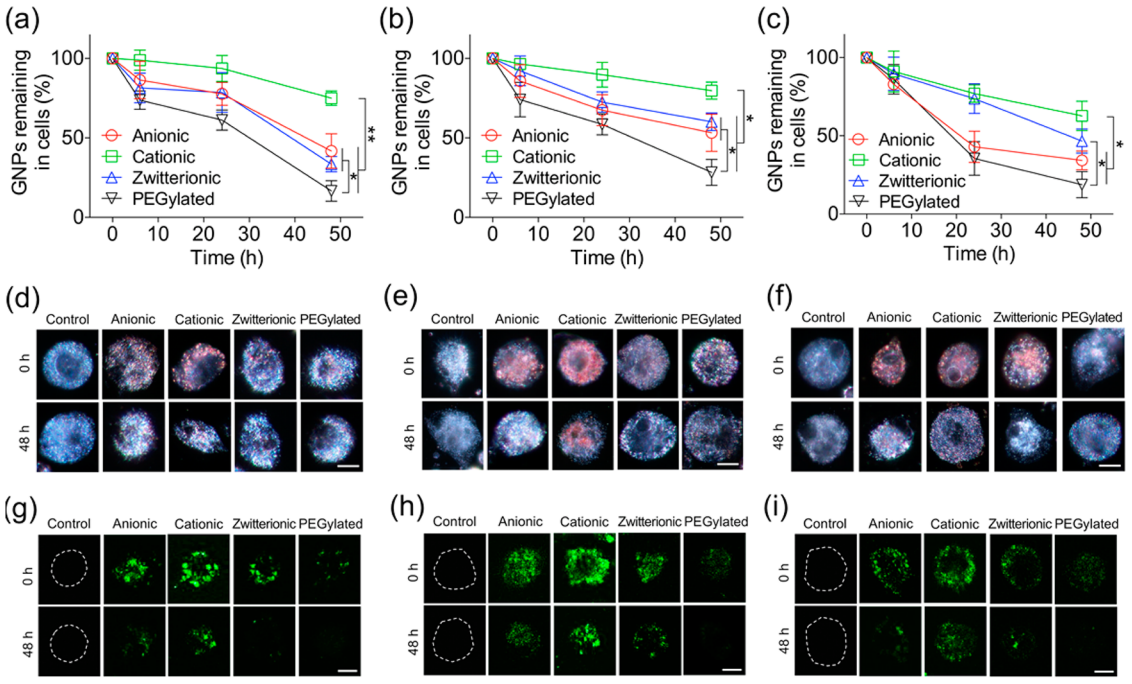


**Figure 3. Exocytosis of serum-coated gold nanoparticles in macrophages. (a–c) Exocytosis rate of serum-coated gold nanoparticles (GNPs) with sizes of 10 (a), 20 (b), and 40 nm (c) in macrophages. Macrophages were treated with serum-coated GNPs for 6 h, washed, and further incubated in the GNP-free media for 6, 24, or 48 h. At each time post-incubation, the supernatant of cells were collected and the amount of GNPs exocytosed from the cells during the incubated period was determined by ICP-MS. (d–f) Dark field microscopic images of serum-coated GNPs with sizes of 10 (d), 20 (e), and 40 nm (f), resident in macrophages at 0 and 48 h postincubation. (g–i) Multiphoton microscopic images of serum-coated GNPs with sizes of 10 (g), 20 (h), and 40 nm (i), resident in macrophages at 0 and 48 h post-incubation. Excitation wavelength at 800 nm was used to image multiphoton luminescence of GNPs, while emission wavelengths ranging from 500 to 650 nm were collected. Scale bars indicate 10 $\mu$m. Data represent means ± SD ($n$ = 3, *$p$ < 0.05 and **$p$ < 0.01 between the data at 48 h, analyzed by two-way analysis of variance, followed by Bonferroni test).**

factor in determining cellular excretion of GNPs smaller than 40 nm. This differs somewhat from a previous report that the exocytosis rate of transferrin-coated GNPs (with diameters of 14–100 nm in cancer cells) is proportional to their size.[31] Specific ligand–receptor interactions play critical roles in mediating the exocytosis of transferrin-coated GNPs, whereas nonspecific interactions between coated serum proteins and plasma membranes seem to be mainly responsible for the exocytosis of serum-coated GNPs here.

Exocytosis patterns were also visualized using both DFM and multiphoton excitation microscopy. Particularly, intrinsic multiphoton luminescence of GNPs allowed clear visualization of their intracellular fate.[68,69] The DFM and multiphoton microscopic images at 48-h post-incubation revealed more orange-red dots, indicating the formation of aggregated GNPs and stronger luminescence signals were observed in cells treated with cationic GNPs, respectively, compared with those treated with other formulations (Figure 3d–i and Supporting Information Figure S6), supporting the ICP-MS results. Importantly, the multiphoton microscopic images revealed that the luminescence signals of intracellular GNPs in the perinuclear regions decreased over time, suggesting that they were indeed exocytosed from the cytoplasm, presumably after passing through lysosomes. Lastly, the GNP treatment did not induce any significant cytotoxicity within the tested exocytosis time period (Supporting Information Figure S7). Together, these results suggest that the surface properties of GNPs, prior to serum coating, also play a primary role in determining their exocytosis fate in macrophages.

Lastly, we further investigated the intracellular fates of 20 nm cationic and PEGylated GNPs in macrophages, due to the dramatic difference in their exocytosis rates. We first observed their exocytosis processes using TEM: the GNP-treated macrophages were incubated in GNP-free media for 24 or 48 h, fixed, sliced, and visualized using TEM. Immediately after the 6-h treatment, most of the cationic GNPs appeared agglomerated in the endosomes, while PEGylated GNPs were observed in the cytoplasm, in the form of individual particles (Figures 4a–d). During exocytosis, large agglomerates of cationic GNPs enclosed in the vesicles appeared to migrate slowly in the cytoplasm, and were then excreted from the cell by lysosomal fusion with the plasma membrane. In contrast, individual PEGylated GNPs, either trapped in the vesicles or in the cytosol, were more likely to move rapidly toward the plasma membrane, without agglomeration, and exit the cell, presumably *via* diffusion. Gel electrophoresis results with proteins eluted from the exocytosed GNPs

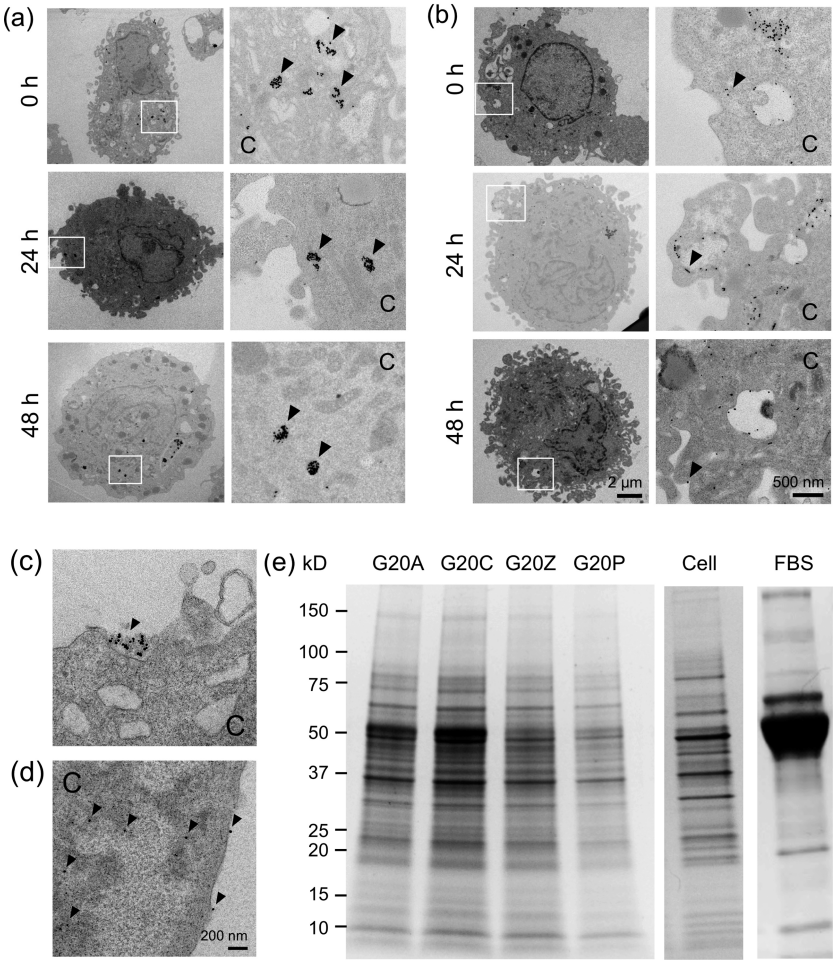


**Figure 4. Exocytosis processes of 20 nm cationic and PEGylated gold nanoparticles. (a and b) Transmission electron microscopic (TEM) images of exocytosis process of serum-coated cationic (a) or PEGylated (b) gold nanoparticles (GNPs) in macrophages. Macrophages were treated with serum-coated GNPs, washed, and further incubated in the GNP-free media for 24 or 48 h. At each time post-incubation, the cells were collected, fixed, and examined by TEM to visualize the exocytosis process of intracellular GNPs. The magnified images on the right side come from the squares in the corresponding images on the left side. (c and d) TEM images showing the exocytosis of serum-coated cationic (c) or PEGylated GNPs (d). GNPs from the plasma membrane of macrophages. (e) Coomassie blue-stained gel staining of GNPs exocytosed from macrophages. At 48 h post-incubation; the exocytosed GNPs were collected from the supernatant by centrifugation. The proteins were eluted from the nanoparticles in sample loading buffer and separated by gel electrophoresis. Untreated cell lysates and 0.5% FBS were used as controls. The number after the G (GNP identifier) designates the size. The letters A, C, Z, and P indicate anionic, cationic, zwitterionic, and PEGylated surface, respectively. Arrow heads and C indicate GNPs and cytoplasm, respectively.**

revealed that the PEGylated GNPs were likely to interact with fewer intracellular proteins during the exocytosis process, compared with cationic GNPs (Figure 4e). It was previously reported that the binding stability between nanoparticles and intracellular proteins could enhance the intracellular retention of nanoparticles.[70] Thus, these results suggest that the PEG coating may mitigate interactions between GNPs and intracellular proteins, thereby facilitating exocytosis. TEM images of GNPs excreted to the media, 48-h post-incubation, exhibited many cationic GNP agglomerates in the extracellular solution, whereas the exocytosed PEGylated GNPs were in the form of individual particles (Supporting Information Figure S8). The broadened absorption spectrum of exocytosed cationic GNPs also indicated their agglomeration, supporting the TEM results (Supporting Information Figure S9). Additionally, no exocytosed membrane vesicles enclosing the GNPs were observed in the TEM images of either formulation, which is different from previous observations.[38,71]

We also investigated whether the initial intracellular concentration of GNPs would influence their exocytosis rate (8006153 particles/cell for cationic GNPs *versus* 898585 particles/cell for PEGylated GNPs; Figure 2b). The initial concentration of cationic GNPs in the cells treated at gold ion concentrations of 15 $\mu$M Au was similar to that of PEGylated GNPs in the cells treated at 150 $\mu$M Au (Supporting Information Figure S10a). Neither did cationic GNPs (15 and 150 $\mu$M Au) exhibit a significant difference in exocytosis rate, although the initial intracellular concentration in the cells treated at 150 $\mu$M Au was $\sim 8\times$ higher than in that in cells treated at 15 $\mu$M Au (Supporting Information Figure S10b). Thus, the exocytosis of PEGylated GNPs was faster than that of

cationic GNPs, even at similar initial intracellular GNP concentrations. Additionally, it was found that the exocytosis rate of PEGylated GNPs was similar to that of PEGylated gold nanorods (GNR) with aspect ratio of ~4.6 (Supporting Information Figure S11), indicating that the exocytosis pattern of PEGylated GNPs is not significantly influenced by their shape. These results confirm that the exocytosis pattern of GNPs is indeed dependent on their native surface properties.

## CONCLUSIONS

In summary, we demonstrated that the native surface chemistries of GNPs and their subsequent opsonization by serum proteins play a critical role in the exocytosis patterns in macrophages. The cationic GNPs were retained in the cells for a relatively long time, while the PEGylated GNPs exhibited the highest exocytosis rate. Intracellular agglomeration of cationic GNPs seemed to delay their exocytosis, whereas PEGylated GNPs, migrating in the cytoplasm in the form of individual particles, were excreted rapidly. We also observed that the exocytosis pattern of GNPs was not significantly governed by their size, particularly in the range from 10 to 40 nm. Although *in vivo* systematic work is still required, our findings suggest that exocytosis of GNPs in the macrophages and their subsequent systemic excretion could be modulated by engineering their surface chemistries. Currently, we are investigating the detailed intracellular molecular mechanisms governing the complex exocytosis process of GNPs in macrophages. We believe that the results of the present study demonstrate promising possibilities for the clinical translation of gold-based nanomaterials.

## MATERIALS AND METHODS

**Preparation of Gold Nanoparticles.** Citrate-capped gold nanoparticles (GNPs) with averages sizes of ~10, 20, and 40 nm were synthesized using previously established method[53] and were used as anionic GNPs. Briefly, 20 mL of 1.0 mM $HAuCl_4 \cdot 3H_2O$ (Sigma) was brought to a boil in a 100 mL bottle and 2.0, 1.6, or 1.0 mL of 38.8 mM trisodium citrate (Sigma) was added for 10, 20, or 40 nm GNPs, respectively. The color of mixture solution changed from yellow to dark red over 5 min. After a boiling and stirring period of 15 min, the GNP solution was kept under room temperature. Zwitterionic and PEGylated GNPs were prepared by coating the citrated GNPs with cysteine and mPEG-sulfhydryl (2k) molecules, respectively. Briefly, for zwitterionic and PEGylated GNPs, 1 mL of 150 $\mu$M Au citrated-capped GNPs was mixed with 70 $\mu$L of 0.001 M L-cysteine (Sigma) and 25 mg of mPEG(2K)-SH (Sunbio, South Korea), respectively. The mixture was vortexed under room temperature overnight. On the other hand, cysteamine-coated GNPs with averages sizes of ~10, 20, and 40 nm were directly synthesized for cationic GNPs using different methods from those used for citrated-coated GNPs.[54,55] For cystamine-coated GNPs with a diameter of 10 nm, 400 $\mu$L of 84.5 $\mu$M cysteamine (Sigma) was added to 40 mL of 1.4 mM $HAuCl_4$ solution. After a stirring period of 20 min, 1 mL of 1 mM $NaBH_4$ solution was added dropwise for 2 min. The mixture was stirred for 12 h at room temperature. For larger cystamine-coated GNPs, 400 $\mu$L of 213 mM cysteamine was added to 40 mL of 1.42 mM $HAuCl_4$ solution. After a stirring period of 20 min at room temperature, 10 or 30 $\mu$L of 10 mM $NaBH_4$ solution was added to the mixture for cysteamine-coated GNPs with diameters of 20 or 40 nm, respectively. The mixture was vigorously stirred for 25 min at room temperature. To remove free organic chemicals, the solution was dialyzed against ultrapure water. For PEGylated gold nanorods (GNR) with aspect ratio of ~4.6, the seed solution was prepared by mixing 5 mL of 0.2 M cetyltrimethylammonium bromide (CTAB, Sigma), 5 mL of 0.5 mM $HAuCl_4$ (Sigma), and 0.6 mL of 0.01 M $NaBH_4$ (Sigma) and aged for 2 h. To grow the seed into the rod shape, 12 $\mu$L of seed solution was mixed with 5 mL of 0.2 M CTAB, 5 mL of 1 mM $HAuCl_4$, 250 $\mu$L of 4 mM $AgNO_3$, and 70 $\mu$L of 78.84 mM ascorbic acid at 25 °C. The synthesized GNRs were washed by centrifugation at 10 000 rpm for 10 min, resuspended in ultrapure water, and coated with 3 mg/mL of mPEG(5K)-SH. For serum coating, all GNP formulations were incubated with 10% fetal bovine serum (FBS) solution (in ultrapure water) for 1 h at room temperature and then washed to remove unbound serum proteins by repeated centrifugation at 12 000 rpm for 30 min. The serum-coated GNPs were finally resuspended in 1 mL of phosphate-buffered saline (PBS).

**Characterization of Gold Nanoparticles.** The absorption spectra were characterized with UV/vis spectrometry (Molecular Devices). The size and morphology were observed with a field emission-transmission electron microscope (FE-TEM, JEOL). The hydrodynamic size and zeta potential were measured at 25 °C using a dynamic light scattering (DLS) instrument (Malvern Instruments). To test colloidal stability of serum-coated GNPs in the physiological condition, the hydrodynamic size and absorption spectrum were monitored hourly for 6 h in serum-free media at 37 °C using DLS instrument and UV/vis spectrometer, respectively. To identify the serum proteins adsorbed on the GNP surface, the serum proteins were eluted from the GNPs in the sample loading buffer (80 mM SDS, 75 $\mu$M SDS, 1.25% $\beta$-mercaptoethanol, 10% glycerol, and 62.5 mM Tris-HCl, pH 6.8) by heating to 95 °C for 5 min and separated by running SDS polyacrylamide gel electrophoresis (SDS-PAGE) at 200 V for 30 min. Finally, the eluted serum proteins were visualized by staining the gel with Coomassie brilliant blue R-250. A total of 0.5% FBS was used as a control. To quantify the serum proteins adsorbed on the surface of GNPs, the serum-coated GNPs were analyzed by thermogravimetric analysis (TGA, TG 209 F3, NETZSCH). Protein analysis was performed from room temperature to 800 °C at a heating rate of 10 °C/min under nitrogen atmosphere with a gas flow rate of 30 mL/min.

**Cell Culture.** Monocyte-like undifferentiated U937 cells were maintained in RPMI 1640 medium supplemented with 10% fetal bovine serum and 100 $\mu$g/mL penicillin and streptomycin at 37 °C. For differentiation into macrophages, nonadherent monocyte-like undifferentiated U937 cells were exposed to 40 nM phorbol-12-myristate-13-acetate (PMA) for 72 h. Differentiated U937 cells were maintained by replacement of PMA-containing media every 2−3 days.

**Endocytosis Study.** Monocyte-like undifferentiated and PMA-differentiated U937 cells were seeded at $5.0 \times 10^5$ cells/(mL/well) in 6-well tissue culture plates with ~90% confluence. The cells were treated with each formulation of serum-coated GNPs at an Au concentration of 150 $\mu$M for 6 h in serum-supplemented media at 37 °C to allow sufficient cellular uptake of GNPs, and intensively washed to remove free and any weakly bound GNPs on the plasma membrane. To measure the quantities of GNPs taken up by cells 6 h post-treatment, the GNP-treated cells were collected by centrifugation at 1000 rpm for 5 min and incubated in *aqua regia* for 24 h to dissolve GNPs and organic materials. The amount of Au ions in the cells was then analyzed by inductively coupled plasma mass spectrometry (ICP-MS, Agilent Technologies) and converted to the number of GNPs per cell. The time-dependent cellular uptake of GNPs was also visualized with their scattering property using dark field microscopy.

The microscopy system consisted of an inverted microscope (Ti−U, Nikon) equipped with a dark-field condenser (N.A. 0.8−0.95), a halogen lamp (100 W), and a true-color digital camera (DS-Ri1-U3, Nikon). Dark field microscopic images of monocyte-like undifferentiated and PMA-differentiated U937 cells treated with each GNP formulation were obtained with a 40× objective (N.A. 0.6).

**Exocytosis Study.** PMA-differentiated U937 cells were treated with each formulation of GNPs at an Au ion concentration of 150 $\mu$M for 6 h in serum-supplemented media at 37 °C, intensively washed to remove free and any weakly bound GNPs on the plasma membrane, and further incubated over 48 h in GNP-free serum-supplemented media to induce their exocytosis. To measure the quantities of GNPs exocytosed from the cells, the GNPs in the supernatants at 0, 6, 24, or 48 h post-incubation were collected by centrifugation at 14 000 rpm for 1 h and dissolved in *aqua regia* for 24 h. The amount of Au ions in the supernatants was then analyzed by ICP-MS. The exocytosis pattern was represented by the percentage of GNPs remaining in the macrophages at each time point after incubation in the GNP-free media. The exocytosis of intracellular GNPs in the PMA-differentiated U937 cells was also visualized at each time point using both dark field and multiphoton excitation microscopy. Time-dependent migration of 20 nm cationic and PEGylated GNPs in the cells was observed by TEM (Tecnai G2, FEI). The GNP-treated cells were incubated for 24 or 48 h with GNP-free serum-supplemented media. The cells were pelleted by centrifugation at 1000 rpm for 5 min and fixed with 2.5% glutaraldyhyde (Sigma) for 1 day. The pellet was then incubated in 1% osmium tetroxide ($OsO_4$, Sigma) for 1 h, dehydrated in a series of alcohol, and substituted with 100% prophylene oxide. The cells were then embedded in the solution composed of prophylene oxide and Epon812 for 24 h, and solidified at 70 °C. Finally, the cells are sliced to a thickness of 70 nm and imaged by TEM. The physicochemical properties of exocytosed GNPs at 48 h post-incubation were examined by TEM, UV−vis spectrometry, and gel electrophoresis. The GNP-treated cells were incubated for 48 h with GNP-free serum-supplemented media. The GNPs in the supernatants were collected by centrifugation at 14 000 rpm for 1 h and resuspended in ultrapure water. For TEM, the GNPs were placed on the grid and negatively stained on a drop of 2% phosphotungstic acid (pH 8.0, Sigma) for 30 s for TEM imaging. To identify the serum proteins adsorbed on the surface of exocytosed GNPs, the proteins were eluted from the GNPs in the sample loading buffer (80 mM SDS, 75 $\mu$M SDS, 1.25% $\beta$-mercaptoethanol, 10% glycerol, and 62.5 mM Tris-HCl, pH 6.8) by heating to 95 °C for 5 min and separated by running SDS polyacrylamide gel electrophoresis (SDS-PAGE) at 200 V for 30 min. Finally, the eluted serum proteins were visualized by staining the gel with Coomassie brilliant blue R-250. Untreated cell lysates and 0.5% FBS were used as controls. For untreated cell samples, PMA-differentiated U937 cells were lysed in 100 $\mu$L of RIPA buffer (0.5% sodium deoxycholate, 0.1% SDS, 1% NP40, 5 mM EDTA in TBS, pH 8.0) for 10 min at 4 °C. The cell lysates were centrifuged at 13 000 rpm for 15 min at 4 °C, and the protein concentrations of cell lysates were determined with the BCA protein assay.

**Cytotoxicity Assay.** PMA-differentiated U937 cells were treated with each formulation of GNPs at an Au ion concentration of 150 $\mu$M for 6 h in serum-supplemented media at 37 °C, intensively washed to remove free and any weakly bound GNPs on the plasma membrane, and further incubated for 6, 24, or 48 h in GNP-free serum-supplemented media. The cell viability was examined by the colormetric thiazoly blue tetrazolium bromide (MTT) assay (Sigma).

**Statistics.** Statistical analyses of the data were performed using one- or two-way analysis of variance (ANOVA), followed by Tukey's or Bonferroni test for multiple comparisons, respectively. The *p*-values less than 0.05 were considered statistically significant. All experiments were performed at least three times. All error bars indicate standard deviation (SD).

*Conflict of Interest:* The authors declare no competing financial interest.

*Acknowledgment.* This work was supported by Basic Science Research Program and the Bio & Medical Technology Development Program of the National Research Foundation (NRF) funded by the Ministry of Science, ICT & Future Planning (Grant Nos. NRF-2012R1A1A1011058 and NRF-2012M3A9C6050125), and the National R&D Program for Cancer Control, Ministry for Health and Welfare (Grant No. 1220070), Republic of Korea. The authors thank the Korea Basic Science Institute, Daejeon, Republic of Korea, for assistance with TEM analysis.

*Supporting Information Available:* Additional TEM data; surface chemistry-dependent absorption of serum proteins on GNPs; stability of serum-coated GNPs in the media; time-dependent change of absorption spectra of serum-coated GNPs; dark field microscopic images; cell viability of macrophages data; adsorption spectra; comparison of exocytosis efficiency; exocytosis of serum-coated PEGylated GNRs in macrophages. This material is available free of charge *via* the Internet at http://pubs.acs.org.

## REFERENCES AND NOTES

1. Kim, B. Y. S.; Rutka, J. T.; Chan, W. C. W. Nanomedicine. *N. Engl. J. Med.* **2010**, *363*, 2434–2443.
2. Cheng, Z.; Al Zaki, A.; Hui, J. Z.; Muzykantov, V. R.; Tsourkas, A. Multifunctional Nanoparticles: Cost *versus* Benefit of Adding Targeting and Imaging Capabilities. *Science* **2012**, *338*, 903–910.
3. Choi, H. S.; Liu, W.; Misra, P.; Tanaka, E.; Zimmer, J. P.; Itty Ipe, B.; Bawendi, M. G.; Frangioni, J. V. Renal Clearance of Quantum Dots. *Nat. Biotechnol.* **2007**, *25*, 1165–1170.
4. Cho, W.-S.; Cho, M.; Jeong, J.; Choi, M.; Cho, H.-Y.; Han, B. S.; Kim, S. H.; Kim, H. O.; Lim, Y. T.; Chung, B. H.; *et al.* Acute Toxicity and Pharmacokinetics of 13 nm-Sized PEG-Coated Gold Nanoparticles. *Toxicol. Appl. Pharmacol.* **2009**, *236*, 16–24.
5. Liu, Z.; Davis, C.; Cai, W.; He, L.; Chen, X.; Dai, H. Circulation and Long-Term Fate of Functionalized, Biocompatible Single-Walled Carbon Nanotubes in Mice Probed by Raman Spectroscopy. *Proc. Natl. Acad. Sci. U.S.A.* **2008**, *105*, 1410–1415.
6. von Maltzahn, G.; Park, J.-H.; Agrawal, A.; Bandaru, N. K.; Das, S. K.; Sailor, M. J.; Bhatia, S. N. Computationally Guided Photothermal Tumor Therapy Using Long-Circulating Gold Nanorod Antennas. *Cancer Res.* **2009**, *69*, 3892–3900.
7. Gu, L.; Fang, R. H.; Sailor, M. J.; Park, J.-H. *In Vivo* Clearance and Toxicity of Monodisperse Iron Oxide Nanocrystals. *ACS Nano* **2012**, *6*, 4947–4954.
8. Thakor, A. S.; Luong, R.; Paulmurugan, R.; Lin, F. I.; Kempen, P.; Zavaleta, C.; Chu, P.; Massoud, T. F.; Sinclair, R.; Gambhir, S. S. The Fate and Toxicity of Raman-Active Silica-Gold Nanoparticles in Mice. *Sci. Transl. Med.* **2011**, *3*, 79ra33.
9. Liu, Z.; Cai, W.; He, L.; Nakayama, N.; Chen, K.; Sun, X.; Chen, X.; Dai, H. *In Vivo* Biodistribution and Highly Efficient Tumour Targeting of Carbon Nanotubes in Mice. *Nat. Nanotechnol.* **2007**, *2*, 47–52.
10. Park, J.-H.; von Maltzahn, G.; Zhang, L.; Schwartz, M. P.; Ruoslahti, E.; Bhatia, S. N.; Sailor, M. J. Magnetic Iron Oxide Nanoworms for Tumor Targeting and Imaging. *Adv. Mater.* **2008**, *20*, 1630–1635.
11. Cedervall, T.; Lynch, I.; Lindman, S.; Berggård, T.; Thulin, E.; Nilsson, H.; Dawson, K. A.; Linse, S. Understanding the Nanoparticle−Protein Corona Using Methods to Quantify Exchange Rates and Affinities of Proteins for Nanoparticles. *Proc. Natl. Acad. Sci. U.S.A.* **2007**, *104*, 2050–2055.
12. Lundqvist, M.; Stigler, J.; Elia, G.; Lynch, I.; Cedervall, T.; Dawson, K. A. Nanoparticle Size and Surface Properties Determine the Protein Corona with Possible Implications for Biological Impacts. *Proc. Natl. Acad. Sci. U.S.A.* **2008**, *105*, 14265–14270.
13. Salvati, A.; Pitek, A. S.; Monopoli, M. P.; Prapainop, K.; Bombelli, F. B.; Hristov, D. R.; Kelly, P. M.; Aberg, C.; Mahon, E.; Dawson, K. A. Transferrin-Functionalized Nanoparticles Lose Their Targeting Capabilities When a Biomolecule Corona Adsorbs on the Surface. *Nat. Nanotechnol.* **2013**, *8*, 137–143.
14. Tenzer, S.; Docter, D.; Kuharev, J.; Musyanovych, A.; Fetz, V.; Hecht, R.; Schlenk, F.; Fischer, D.; Kiouptsi, K.; Reinhardt, C.; *et al.* Rapid Formation of Plasma Protein Corona Critically

Affects Nanoparticle Pathophysiology. *Nat. Nanotechnol.* **2013**, *8*, 772–781.
15. Fischer, H. C.; Hauck, T. S.; Gomez-Aristizabal, A.; Chan, W. C. Exploring Primary Liver Macrophages for Studying Quantum Dot Interactions with Biological Systems. *Adv. Mater.* **2010**, *22*, 2520–2524.
16. Park, E.-J.; Park, K. Oxidative Stress and Pro-Inflammatory Responses Induced by Silica Nanoparticles *In Vivo* and *In Vitro*. *Toxicol. Lett.* **2009**, *184*, 18–25.
17. Yu, S. S.; Lau, C. M.; Thomas, S. N.; Jerome, W. G.; Maron, D. J.; Dickerson, J. H.; Hubbell, J. A.; Giorgio, T. D. Size- and Charge-Dependent Non-Specific Uptake of PEGylated Nanoparticles by Macrophages. *Int. J. Nanomed.* **2012**, *7*, 799–813.
18. Walkey, C. D.; Olsen, J. B.; Guo, H.; Emili, A.; Chan, W. C. Nanoparticle Size and Surface Chemistry Determine Serum Protein Adsorption and Macrophage Uptake. *J. Am. Chem. Soc.* **2012**, *134*, 2139–2147.
19. Arnida; Janát-Amsbury, M. M.; Ray, A.; Peterson, C. M.; Ghandehari, H. Geometry and Surface Characteristics of Gold Nanoparticles Influence Their Biodistribution and Uptake by Macrophages. *Eur. J. Pharm. Biopharm.* **2011**, *77*, 417–423.
20. Lunov, O.; Syrovets, T.; Loos, C.; Beil, J.; Delacher, M.; Tron, K.; Nienhaus, G. U.; Musyanovych, A.; Mailänder, V.; Landfester, K.; *et al.* Differential Uptake of Functionalized Polystyrene Nanoparticles by Human Macrophages and a Monocytic Cell Line. *ACS Nano* **2011**, *5*, 1657–1669.
21. Clift, M. J. D.; Rothen-Rutishauser, B.; Brown, D. M.; Duffin, R.; Donaldson, K.; Proudfoot, L.; Guy, K.; Stone, V. The Impact of Different Nanoparticle Surface Chemistry and Size on Uptake and Toxicity in a Murine Macrophage Cell Line. *Toxicol. Appl. Pharmacol.* **2008**, *232*, 418–427.
22. Dykman, L. A.; Khlebtsov, N. G. Uptake of Engineered Gold Nanoparticles into Mammalian Cells. *Chem. Rev.* **2014**, *114*, 1258–1288.
23. Dobrovolskaia, M. A.; McNeil, S. E. Immunological Properties of Engineered Nanomaterials. *Nat. Nanotechnol.* **2007**, *2*, 469–478.
24. Wang, H.; Wu, L.; Reinhard, B. M. Scavenger Receptor Mediated Endocytosis of Silver Nanoparticles into J774A.1 Macrophages Is Heterogeneous. *ACS Nano* **2012**, *6*, 7122–7132.
25. Sakhtianchi, R.; Minchin, R. F.; Lee, K.-B.; Alkilany, A. M.; Serpooshan, V.; Mahmoudi, M. Exocytosis of Nanoparticles from Cells: Role in Cellular Retention and Toxicity. *Adv. Colloid Interface Sci.* **2013**, *201−202*, 18–29.
26. Furumoto, K.; Ogawara, K.-i.; Yoshida, M.; Takakura, Y.; Hashida, M.; Higaki, K.; Kimura, T. Biliary Excretion of Polystyrene Microspheres Depends on the Type of Receptor-Mediated Uptake in Rat Liver. *Biochim. Biophys. Acta, Gen. Subj.* **2001**, *1526*, 221–226.
27. Souris, J. S.; Lee, C.-H.; Cheng, S.-H.; Chen, C.-T.; Yang, C.-S.; Ho, J.-a. A.; Mou, C.-Y.; Lo, L.-W. Surface Charge-Mediated Rapid Hepatobiliary Excretion of Mesoporous Silica Nanoparticles. *Biomaterials* **2010**, *31*, 5564–5574.
28. Panyam, J.; Labhasetwar, V. Dynamics of Endocytosis and Exocytosis of Poly(D,L-lactide-*co*-glycolide) Nanoparticles in Vascular Smooth Muscle Cells. *Pharm. Res.* **2003**, *20*, 212–220.
29. Dombu, C. Y.; Kroubi, M.; Zibouche, R.; Matran, R.; Betbeder, D. Characterization of Endocytosis and Exocytosis of Cationic Nanoparticles in Airway Epithelium Cells. *Nanotechnology* **2010**, *21*, 355102.
30. Park, J. S.; Han, T. H.; Lee, K. Y.; Han, S. S.; Hwang, J. J.; Moon, D. H.; Kim, S. Y.; Cho, Y. W. N-acetyl histidine-Conjugated Glycol Chitosan Self-Assembled Nanoparticles for Intracytoplasmic Delivery of Drugs: Endocytosis, Exocytosis and Drug Release. *J. Controlled Release* **2006**, *115*, 37–45.
31. Chithrani, B. D.; Chan, W. C. Elucidating the Mechanism of Cellular Uptake and Removal of Protein-Coated Gold Nanoparticles of Different Sizes and Shapes. *Nano Lett.* **2007**, *7*, 1542–1550.
32. Bartczak, D.; Nitti, S.; Millar, T. M.; Kanaras, A. G. Exocytosis of Peptide Functionalized Gold Nanoparticles in Endothelial Cells. *Nanoscale* **2012**, *4*, 4470–4472.
33. Chen, R.; Huang, G.; Ke, P. C. Calcium-Enhanced Exocytosis of Gold Nanoparticles. *Appl. Phys. Lett.* **2010**, *97*, 093706.
34. Cho, E. C.; Zhang, Y.; Cai, X.; Moran, C. M.; Wang, L. V.; Xia, Y. Quantitative Analysis of the Fate of Gold Nanocages In Vitro and In Vivo after Uptake by U87-MG Tumor Cells. *Angew. Chem., Int. Ed.* **2013**, *52*, 1152–1155.
35. Kim, C. S.; Le, N. D. B.; Xing, Y.; Yan, B.; Tonga, G. Y.; Kim, C.; Vachet, R. W.; Rotello, V. M. The Role of Surface Functionality in Nanoparticle Exocytosis. *Adv. Healthcare Mater.* **2014**, DOI: 10.1002/adhm.201400001.
36. Jin, H.; Heller, D. A.; Sharma, R.; Strano, M. S. Size-Dependent Cellular Uptake and Expulsion of Single-Walled Carbon Nanotubes: Single Particle Tracking and a Generic Uptake Model for Nanoparticles. *ACS Nano* **2009**, *3*, 149–158.
37. Jin, H.; Heller, D. A.; Strano, M. S. Single-Particle Tracking of Endocytosis and Exocytosis of Single-Walled Carbon Nanotubes in NIH-3T3 Cells. *Nano Lett.* **2008**, *8*, 1577–1585.
38. Serda, R. E.; Mack, A.; van de Ven, A. L.; Ferrati, S.; Dunner, K., Jr.; Godin, B.; Chiappini, C.; Landry, M.; Brousseau, L.; Liu, X.; *et al.* Logic-Embedded Vectors for Intracellular Partitioning, Endosomal Escape, and Exocytosis of Nanoparticles. *Small* **2010**, *6*, 2691–2700.
39. Wang, Y.; Wu, Q.; Sui, K.; Chen, X.-X.; Fang, J.; Hu, X.; Wu, M.; Liu, Y. A Quantitative Study of Exocytosis of Titanium Dioxide Nanoparticles from Neural Stem Cells. *Nanoscale* **2013**, *5*, 4737–4743.
40. Ruan, G.; Agrawal, A.; Marcus, A. I.; Nie, S. Imaging and Tracking of Tat Peptide-Conjugated Quantum Dots in Living Cells: New Insights into Nanoparticle Uptake, Intracellular Transport, and Vesicle Shedding. *J. Am. Chem. Soc.* **2007**, *129*, 14759–14766.
41. Jiang, X.; Rocker, C.; Hafner, M.; Brandholt, S.; Dorlich, R. M.; Nienhaus, G. U. Endo- and Exocytosis of Zwitterionic Quantum Dot Nanoparticles by Live HeLa Cells. *ACS Nano* **2010**, *4*, 6787–6797.
42. Ohta, S.; Inasawa, S.; Yamaguchi, Y. Real Time Observation and Kinetic Modeling of the Cellular Uptake and Removal of Silicon Quantum Dots. *Biomaterials* **2012**, *33*, 4639–4645.
43. Slowing, I. I.; Vivero-Escoto, J. L.; Zhao, Y.; Kandel, K.; Peeraphatdit, C.; Trewyn, B. G.; Lin, V. S. Y. Exocytosis of Mesoporous Silica Nanoparticles from Mammalian Cells: From Asymmetric Cell-to-Cell Transfer to Protein Harvesting. *Small* **2011**, *7*, 1526–1532.
44. Yanes, R. E.; Tarn, D.; Hwang, A. A.; Ferris, D. P.; Sherman, S. P.; Thomas, C. R.; Lu, J.; Pyle, A. D.; Zink, J. I.; Tamanoi, F. Involvement of Lysosomal Exocytosis in the Excretion of Mesoporous Silica Nanoparticles and Enhancement of the Drug Delivery Effect by Exocytosis Inhibition. *Small* **2013**, *9*, 697–704.
45. Fang, C.-Y.; Vaijayanthimala, V.; Cheng, C.-A.; Yeh, S.-H.; Chang, C.-F.; Li, C.-L.; Chang, H.-C. The Exocytosis of Fluorescent Nanodiamond and Its Use as a Long-Term Cell Tracker. *Small* **2011**, *7*, 3363–3370.
46. Pincus, T.; Ferraccioli, G.; Sokka, T.; Larsen, A.; Rau, R.; Kushner, I.; Wolfe, F. Evidence from Clinical Trials and Long-Term Observational Studies that Disease-Modifying Anti-Rheumatic Drugs Slow Radiographic Progression in Rheumatoid Arthritis: Updating a 1983 Review. *Rheumatology* **2002**, *41*, 1346–1356.
47. Chithrani, B. D.; Ghazani, A. A.; Chan, W. C. Determining the Size and Shape Dependence of Gold Nanoparticle Uptake into Mammalian Cells. *Nano Lett.* **2006**, *6*, 662–668.
48. Jiang, W.; Kim, B. Y.; Rutka, J. T.; Chan, W. C. Nanoparticle-Mediated Cellular Response is Size-Dependent. *Nat. Nanotechnol.* **2008**, *3*, 145–150.
49. Albanese, A.; Chan, W. C. Effect of Gold Nanoparticle Aggregation on Cell Uptake and Toxicity. *ACS Nano* **2011**, *5*, 5478–5489.
50. Marchesano, V.; Hernandez, Y.; Salvenmoser, W.; Ambrosone, A.; Tino, A.; Hobmayer, B.; M. de la Fuente, J.; Tortiglione, C. Imaging Inward and Outward Trafficking of Gold Nanoparticles in Whole Animals. *ACS Nano* **2013**, *7*, 2431–2442.

51. Sadauskas, E.; Danscher, G.; Stoltenberg, M.; Vogel, U.; Larsen, A.; Wallin, H. Protracted Elimination of Gold Nanoparticles from Mouse Liver. *Nanomed. Nanotechnol. Biol. Med.* **2009**, *5*, 162–169.
52. Goel, R.; Shah, N.; Visaria, R.; Paciotti, G. F.; Bischof, J. C. Biodistribution of TNF-α-Coated Gold Nanoparticles in an *in vivo* Model System. *Nanomedicine* **2009**, *4*, 401–410.
53. Grabar, K. C.; Freeman, R. G.; Hommer, M. B.; Natan, M. J. Preparation and Characterization of Au Colloid Monolayers. *Anal. Chem.* **1995**, *67*, 735–743.
54. Lee, S. H.; Bae, K. H.; Kim, S. H.; Lee, K. R.; Park, T. G. Amine-Functionalized Gold Nanoparticles as Non-Cytotoxic and Efficient Intracellular siRNA Delivery Carriers. *Int. J. Pharm.* **2008**, *364*, 94–101.
55. Jv, Y.; Li, B.; Cao, R. Positively-Charged Gold Nanoparticles as Peroxidiase Mimic and Their Application in Hydrogen Peroxide and Glucose Detection. *Chem. Commun.* **2010**, *46*, 8017–8019.
56. Ehrenberg, M. S.; Friedman, A. E.; Finkelstein, J. N.; Oberdörster, G.; McGrath, J. L. The Influence of Protein Adsorption on Nanoparticle Association with Cultured Endothelial Cells. *Biomaterials* **2009**, *30*, 603–610.
57. Thomas, S. N.; van der Vlies, A. J.; O'Neil, C. P.; Reddy, S. T.; Yu, S. S.; Giorgio, T. D.; Swartz, M. A.; Hubbell, J. A. Engineering Complement Activation on Polypropylene Sulfide Vaccine Nanoparticles. *Biomaterials* **2011**, *32*, 2194–2203.
58. Gref, R.; Lück, M.; Quellec, P.; Marchand, M.; Dellacherie, E.; Harnisch, S.; Blunk, T.; Müller, R. H. 'Stealth' Corona-Core Nanoparticles Surface Modified by Polyethylene Glycol (PEG): Influences of the Corona (PEG Chain Length and Surface Density) and of the Core Composition on Phagocytic Uptake and Plasma Protein Adsorption. *Colloids Surf., B* **2000**, *18*, 301–313.
59. Choi, H. S.; Ashitate, Y.; Lee, J. H.; Kim, S. H.; Matsui, A.; Insin, N.; Bawendi, M. G.; Semmler-Behnke, M.; Frangioni, J. V.; Tsuda, A. Rapid Translocation of Nanoparticles from the Lung Airspaces to the Body. *Nat. Biotechnol.* **2010**, *28*, 1300–1303.
60. Weissleder, R.; Kelly, K.; Sun, E. Y.; Shtatland, T.; Josephson, L. Cell-Specific Targeting of Nanoparticles by Multivalent Attachment of Small Molecules. *Nat. Biotechnol.* **2005**, *23*, 1418–1423.
61. Wang, X.-b.; Gao, H.-y.; Hou, B.-l.; Huang, J.; Xi, R.-g.; Wu, L.-j. Nanoparticle Realgar Powders Induce Apoptosis in U937 Cells through Caspase MAPK and Mitochondrial Pathways. *Arch. Pharm. Res.* **2007**, *30*, 653–658.
62. Zhu, M.-T.; Wang, B.; Wang, Y.; Yuan, L.; Wang, H.-J.; Wang, M.; Ouyang, H.; Chai, Z.-F.; Feng, W.-Y.; Zhao, Y.-L. Endothelial Dysfunction and Inflammation Induced by Iron Oxide Nanoparticle Exposure: Risk Factors for Early Atherosclerosis. *Toxicol. Lett.* **2011**, *203*, 162–171.
63. Ting, S. R. S.; Whitelock, J. M.; Tomic, R.; Gunawan, C.; Teoh, W. Y.; Amal, R.; Lord, M. S. Cellular Uptake and Activity of Heparin Functionalised Cerium Oxide Nanoparticles in Monocytes. *Biomaterials* **2013**, *34*, 4377–4386.
64. Lord, M. S.; Jung, M.; Teoh, W. Y.; Gunawan, C.; Vassie, J. A.; Amal, R.; Whitelock, J. M. Cellular Uptake and Reactive Oxygen Species Modulation of Cerium Oxide Nanoparticles in Human Monocyte Cell Line U937. *Biomaterials* **2012**, *33*, 7915–7924.
65. Aaron, J.; Travis, K.; Harrison, N.; Sokolov, K. Dynamic Imaging of Molecular Assemblies in Live Cells Based on Nanoparticle Plasmon Resonance Coupling. *Nano Lett.* **2009**, *9*, 3612–3618.
66. Moghimi, S. M.; Hunter, A. C.; Murray, J. C. Long-Circulating and Target-Specific Nanoparticles: Theory to Practice. *Pharmacol. Rev.* **2001**, *53*, 283–318.
67. Sadauskas, E.; Wallin, H.; Stoltenberg, M.; Vogel, U.; Doering, P.; Larsen, A.; Danscher, G. Kupffer Cells are Central in the Removal of Nanoparticles from the Organism. *Part. Fibre Toxicol.* **2007**, *4*, 10.
68. Farrer, R. A.; Butterfield, F. L.; Chen, V. W.; Fourkas, J. T. Highly Efficient Multiphoton-Absorption-Induced Luminescence from Gold Nanoparticles. *Nano Lett.* **2005**, *5*, 1139–1142.
69. Dowling, M. B.; Li, L.; Park, J.; Kumi, G.; Nan, A.; Ghandehari, H.; Fourkas, J. T.; DeShong, P. Multiphoton-Absorption-Induced-Luminescence (MAIL) Imaging of Tumor-Targeted Gold Nanoparticles. *Bioconjugate Chem.* **2010**, *21*, 1968–1977.
70. Wu, L.-C.; Chu, L.-W.; Lo, L.-W.; Liao, Y.-C.; Wang, Y.-C.; Yang, C.-S. Programmable Cellular Retention of Nanoparticles by Replacing the Synergistic Anion of Transferrin. *ACS Nano* **2012**, *7*, 365–375.
71. Chu, Z.; Huang, Y.; Tao, Q.; Li, Q. Cellular Uptake, Evolution, and Excretion of Silica Nanoparticles in Human Cells. *Nanoscale* **2011**, *3*, 3291–3299.